Journal of Physics: Conference Series

PAPER • **OPEN ACCESS**

Effect of TiO_2 addition on phase stability and sintering behavior of 1 mol%La_2O_3 -2 mol%Gd_2O_3-2 mol%Yb_2O_3-6 mol%Y_2O_3 co-doped ZrO_2

To cite this article: Li Li *et al* 2022 *J. Phys.: Conf. Ser.* **2383** 012122

Effect of TiO_2 addition on phase stability and sintering behavior of 1 mol%La_2O_3 -2 mol%Gd_2O_3-2 mol%Yb_2O_3-6 mol%Y_2O_3 co-doped ZrO_2

Li Li[a], Xingeng Lei[b], Quansheng Wang[c], Hanqi Zhao[d], Xianjin Ning[e]

School of Materials Science and Engineering, Beijing Institute of Technology, Beijing, 100081, China

[a]lil7399@foxmail.com, [b]xglei80@163.com, [c]qsh_wang@bit.edu.cn, [d]254312448@qq.com, [e]nxj@bit.edu.cn

Abstract: In this study, 1 mol%La_2O_3-2 mol%Gd_2O_3-2 mol%Yb_2O_3-6 mol%Y_2O_3 co-doped ZrO_2 (LGYYSZ) with 0 mol%, 5 mol% and 10 mol% TiO_2 additions were synthesised by solid-state reactions. The effect of TiO_2 addition on the phase stability of LGYYSZ and its sintering behaviour at 1500 °C were investigated using XRD, SEM and EDS. The results show that the eutectic temperature of LGYYSZ decreases with increasing TiO_2 content. SEM, EDS and XRD results show that the TiO_2 addition is reacted with the La_2O_3 in LGYYSZ to form a orthorhombic $La_2Ti_2O_7$ phase. When held at 1500 °C, $La_2Ti_2O_7$ is precipitated on the surface of the samples by evaporation-condensation mechanism. This resulted in the anti-sintering properties of LGYYSZ at 1500 °C decreasing with increasing TiO_2 content.

1. Introduction

Thermal barrier coatings (TBCs) are now being used to provide thermal insulation to metallic components from the hot gas stream in gas-turbine engines. At present, the widely used ceramic thermal barrier coating material is 7-8 wt% Y_2O_3 partially stabilized zirconia (PYSZ) [1]. PYSZ coating prepared by APS or EB-PVD consists of a single metastable tetragonal prime phase (t'), this phase has high fracture toughness due to its ferroelastic toughening property. However, above 1200 °C, the metastable t' phase of PYSZ decomposes into equilibrium tetragonal (t) and cubic (c) phases by diffusion [2-5], and then, the equilibrium t phase transforms to monoclinic (m) phase during cooling resulting in volume expansion and premature coating failure. Therefore, it is desirable to discover new TBCs metarials that can be used at higer temperature. Many studies have shown that the addition of more yttria or rare-earth oxide stabilizers will result in a completely stable cubic phase ZrO_2, which does not undergo phase changes and has a lower thermal conductivity than PYSZ [6-9]. In our previous study [10], a La_2O_3-Gd_2O_3-Yb_2O_3-Y_2O_3 co-doped cubic ZrO_2 (LGYYSZ) material was synthesized by solid reaction method. Compared to PYSZ, LGYYSZ shows good sintering resistance and excellent phase stability which makes it a potential material for ceramic thermal barrier coating that can be applied at 1500 °C. However, cubic phase ZrO_2 coatings exhibit poor thermal cycle life in tests that correlate with its poor mechanical properties [11, 12].

To improve the mechanical properties of cubic phase ZrO_2 materials, many studies has been made to find newer doped oxides. TiO_2 is an effective additive for improving mechanical properties of yttria-stabilized ZrO_2, such as toughness, tensile and compressive properties at high temperatures [13-17]. Zhu et al. [18] pointed out that the furnace cyclic life of a Gd_2O_3-Yb_2O_3-Y_2O_3 co-doped cubic ZrO_2 TBC can

be effectively improved with the addition of 10 mol% TiO_2. However, there are no reports of the coating sintering behavior at higher than 1200 ℃. Moreover, there are rarely reported studies on the effect of TiO_2 doping on the phase structure for quaternary or higher order systems.

In this study, LGYYSZ doped with 0-10 mol%TiO_2 was prepared using a solid-state reaction method. The effects of the TiO_2 doping content on the phase stability and sintering resistance of LGYYSZ at 1500 ℃ were investigated.

2. Experimental

In this study, 1 mol%La_2O_3-2 mol%Gd_2O_3-2 mol%Yb_2O_3-6 mol%Y_2O_3 co-doped ZrO_2 (LGYYSZ) with 0, 5 and 10 mol% TiO_2 additions were synthesised by solid-state reactions, noted as 0Ti, 5Ti and 10Ti, respectively.

Commercial La_2O_3, Gd_2O_3, Yb_2O_3, Y_2O_3, ZrO_2, and TiO_2 powders (purity≥99.9%, 1-3 μm, ENO material, Co., Ltd., Qinhuangdao, China) were used for samples preparation. According to their stoichiometric ratio, all powders were weighted and mixed by planetary ball milling (350 rpm, 12 h) in ethanol. After that, the mixtures were dried at 120 ℃ for 10 h in corundum crucibles. Then the mixtures were calcined at 1400 ℃, 1450 ℃, and 1500 ℃ for 4 h, 8 h, and 10 h. In the end, the synthesized materials were ground by planetary ball milling (350 rpm, 24 h) in ethanol and the fine powders were screened using a 200-mesh sieve, and the obtained fine powder was used to prepare the pellets for sintering behavior evaluation.

The phase structures of the as-synthesized powders were analyzed using X-ray diffraction (XRD) by an X-ray diffractometer (Ultima-IV Diffractometer, Rigaku, Japan). The scanning range was 20°- 80° and the scanning rate was 6 °/min. Lattice parameters for the samples at 71-76 ° were determined by slow-scan at a scan rate of 0.2 °/min. 0Ti and 5Ti powders calcined at 1500 ℃ for 10 h and 10Ti powders calcined at 1500 ℃ for 4 h were pressed as disc pellets (diameter: 16 mm, thickness: 2.5 mm) under 3 MPa and then isostatically-pressed at 200 MPa. After that, the pellets were sintered at 1500 ℃ for 4 h, 10 h, and 30 h.

The density of the sintered pellets was measured by the Archimedes method using deionized water, and the diameters of each sintered pellets were measured with a caliper. Microstructure and compositions of sintered pellets were observed by a field emission scanning electron microscope (SEM; Quanta 250 FEG, FEI Company, USA) with an energy-dispersive spectrometer (EDS; XFlash6-30, Bruker, Germany). All sintered pellets were also analyzed by the X-ray diffractometer over the range of 20°- 80°, and the scan rate is 6 °/min.

3. Results and discussion

3.1 Phase structures of powders and sintered pellets

XRD patterns of powders with different TiO_2 content calcined at 1400 ℃ for 4 h were presented in Fig. 1. There is a large amount of monoclinic phase (PDF#78-0047) in 0Ti, and slightly diffraction peaks of monoclinic still can be distinguished in 5Ti. However, the monoclinic phase completely disappeared and the single cubic phase (PDF#30-1648) was obtained in 10Ti. When holding temperature increased to 1450 ℃, no peaks other than those attributable to cubic ZrO_2 were detected in 5Ti, and there was no discernible change even after holding at 1500 ℃ for 10 h (not shown here). While 0Ti was held at 1500 ℃ for no less than 10 h to obtain a single cubic phase structure. Therefore, the doping of TiO_2 significantly reduces eutectic temperature of LGYYSZ.

To investigate the evaluation of new phases in the sintering process, 0Ti and 5Ti powders calcined at 1500 ℃ for 10 h and 10Ti powders calcined at 1500 ℃ for 4 h were used for subsequent pellets sintering studies. All synthesized powders exhibit single cubic phase structure (see Fig. 2). There are no diffraction peaks of TiO_2 in the powders patterns, which means that TiO_2 have solid soluted to ZrO_2 crystal completely. As indicated in Fig. 2(b), the diffraction peak (400) shifted towards higher diffraction angles with increasing TiO_2 content. According to the XRD results, lattice constants of 0Ti, 5Ti, and 10Ti were calculated, see Table 1. It demonstrates that increasing TiO_2 content in LGYYSZ leads to

lattice constant decreases. Hence, Ti^{4+} cation replaces Zr^{4+} cation as a substitution in the lattice, agreeing with previous studies of yttria-stabilized ZrO_2 [19, 20].

XRD patterns of 5Ti and 10Ti pellets sintered at 1500 ℃ for 4 h, 10 h, and 30 h were displayed in Fig. 3. Despite cubic ZrO_2 being observed in all pellets, unlike the synthetic powder, orthorhombic $La_2Ti_2O_7$ (PDF#70-1690) was also observed in the 5Ti pellets sintered for 30 hours and in all 10Ti pellets, having a (010) preferred orientation perpendicular to the surface. And the relative content of $La_2Ti_2O_7$ in the 10Ti pellets gradually decreases with increasing sintering time, see Fig. 3b. This anomaly would be discussed in the following sections combined with SEM and EDS results.

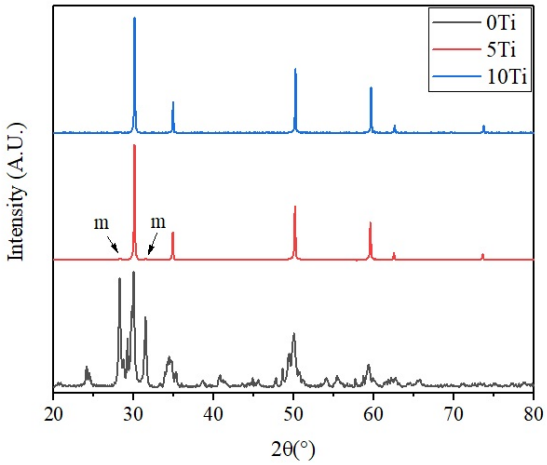

Fig. 1 XRD patterns of 0Ti, 5Ti, and 10Ti powders calcined at 1400 ℃ for 4 h.

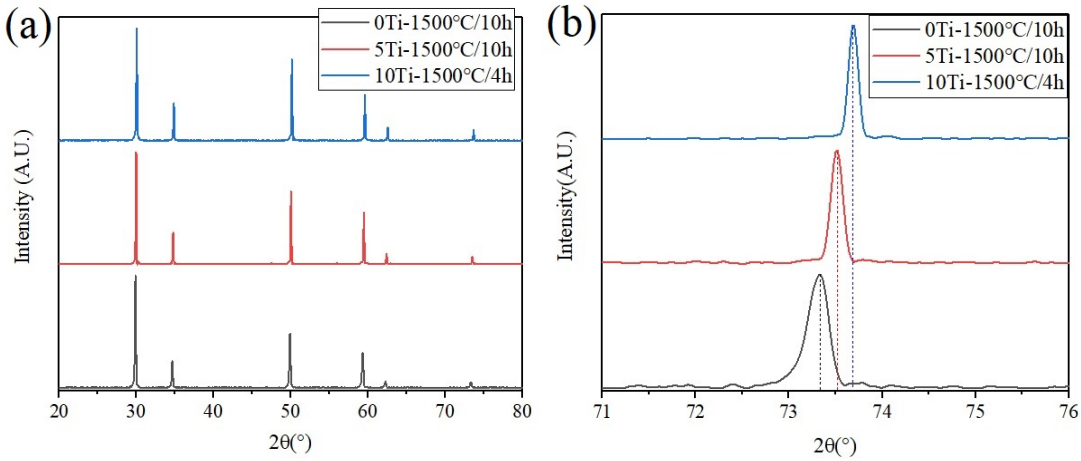

Fig. 2 XRD patterns of 0Ti, 5Ti, 10Ti powders used for sintering test, (a)2θ=20-80°, (b) (400) peak.

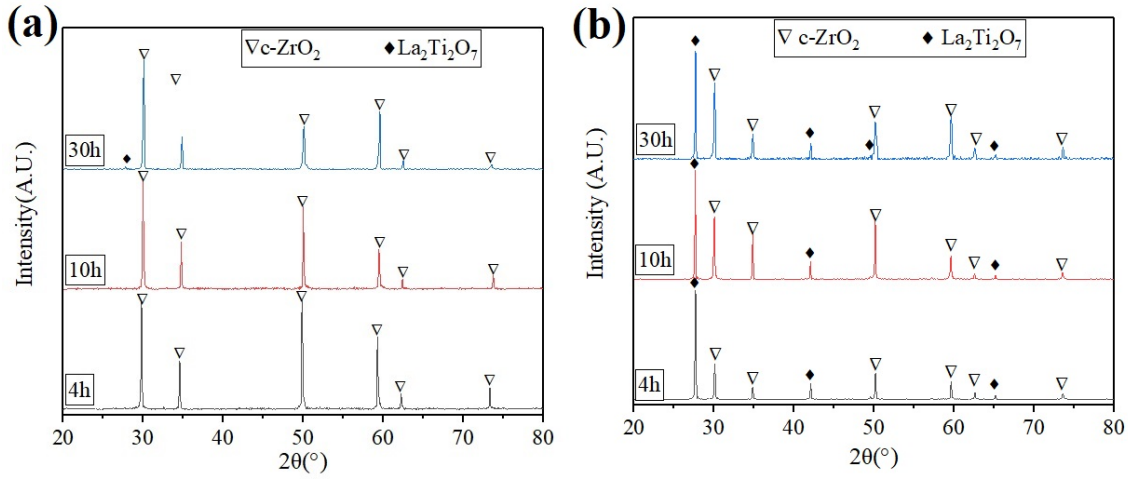

Fig. 3 XRD patterns of 5Ti (a) and 10Ti (b) pellets sintered at 1500 ℃ for 4 h, 10 h, and 30 h.

Table 1. Lattice constant and theoretical density of each compound.

Specimen	lattice constant (Å)	Theoretical density (g/cm^3)
0Ti	5.1597	6.1709
5Ti	5.1482	6.1150
10Ti	5.1386	6.0537

3.2 Porosities and shrinkage rate of sintered pellets

Fig. 4(a) and (b) depicted the variation of porosities and diameter shrinkage ratios of 0Ti, 5Ti, and 10Ti bulk specimens sintered at 1500 ℃ for 4 h, 10 h, and 30 h. The relative density of samples varies from 81.7% to 99.3% due to sintering time and TiO_2 content. The porosities of 0Ti were still more than 12% after sintered at 1500 ℃ for 30 h, shows a very high sintering resistance at this temperature due to the multi-defect clusters caused by multi-rare earth oxides co-doped [10, 11]. The results showed that the densification of LGYYSZ increased and the residual porosity decreased with the increase of TiO_2 addition, it is consistent with the effect of TiO_2 as a sintering aid [21]. As same as porosities, increment TiO_2 amount in LGYYSZ leads to more shrinkage in the bulk specimen, probably due to the reduction of pores in the specimen.

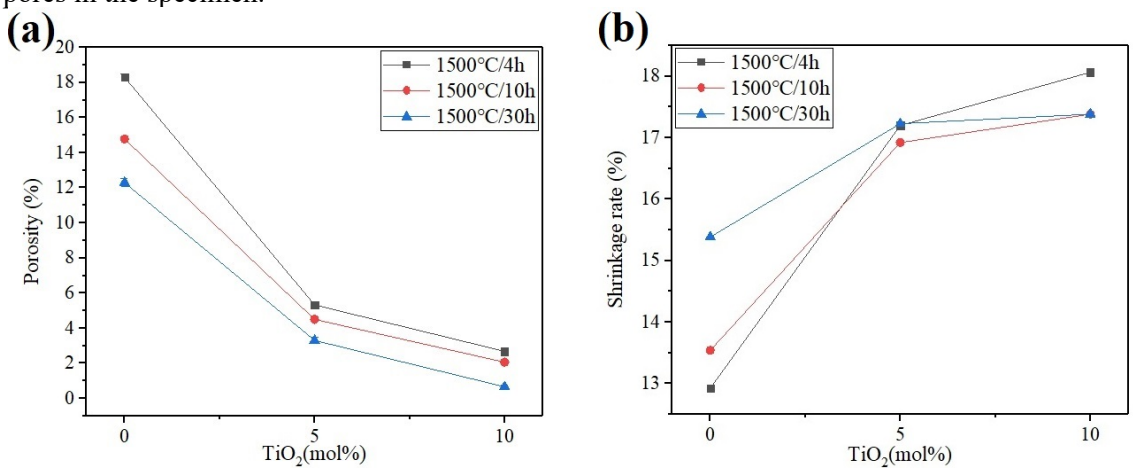

Fig. 4 Porosities (a) and diameter shrinkage ratios (b) of 0Ti, 5Ti, and 10Ti bulk specimens sintered at 1500 ℃ for 4 h, 10 h, and 30 h.

3.3 The Grain size of sintered pellets

The typical cross-section SEM micrographs of 0Ti, 5Ti, and 10Ti bulk specimens sintered at 1500 ℃ for 4 h and 30 h, after polishing and thermally etching, are presented in Fig. 5 (a)-(f), respectively. It can be seen that the grain size of all specimens increases with increasing sintering time. As can be seen from Figs. 5a and 5b, the grain growth of the 0Ti specimens was very slow. Even after 30 h of sintering, the average grain size (3.28 ± 0.22 μm) was still very small. Furthermore, it still retained a large number of intergranular pores and a few of intragranular pores in the pellet (see Fig. 5(b)), concurring with its porosity and shrinkage rate changes (see Fig. 4). All these revealed that the 0Ti pellet still has not reached the late stage of sintering [22]. Fully densified bodies were obtained for 5Ti and 10Ti in comparison with the 0Ti bulk specimen. There were still few intragranular pores in 5Ti and 10Ti after sintered for 30 h, but the large number of intergranular pores observed in 0Ti almost completely disappeared after only 4 h of sintering in these specimens, it seems they were reached the late stage of sintering.

Figure 6(b) shows the variation of the average grain size with the composition of pellet, which indicates that the grain size also increases with the increase of TiO_2 content. Furthermore, the effect of TiO_2 content is more obvious compared to sintering time. This is consistent with what has been reported in the literature [23]. The grain growth of ZrO_2 in the late sintering stage is controlled by the grain boundary mobility, which depends on the diffusion rate of the dopant and the amount of dopant segregation at the grain boundary, whereas in cubic ZrO_2 the effect of dopants segregation on the grain boundary mobility can be neglected [24,25], so the grain boundary mobility of 5Ti and 10Ti was charged by the diffusivity of the dopants. In general, the diffusivity of a dopant is negatively related to its atomic mass and ionic radius. The radii (coordination number:8) and atomic masses of the matrix and dopant elements are provided in Table 2. Compared with the trivalent cations, Ti^{4+} has the smallest radius and smallest atomic mass, so the increase of TiO_2 in LGYYZ leads to higher diffusivity, which results in higher grain boundary mobility and larger grain size.

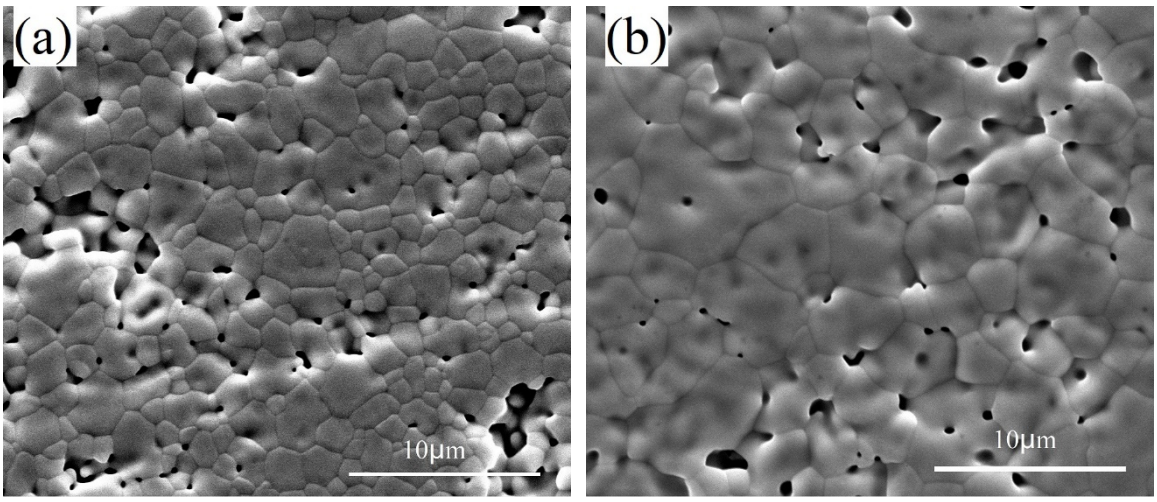

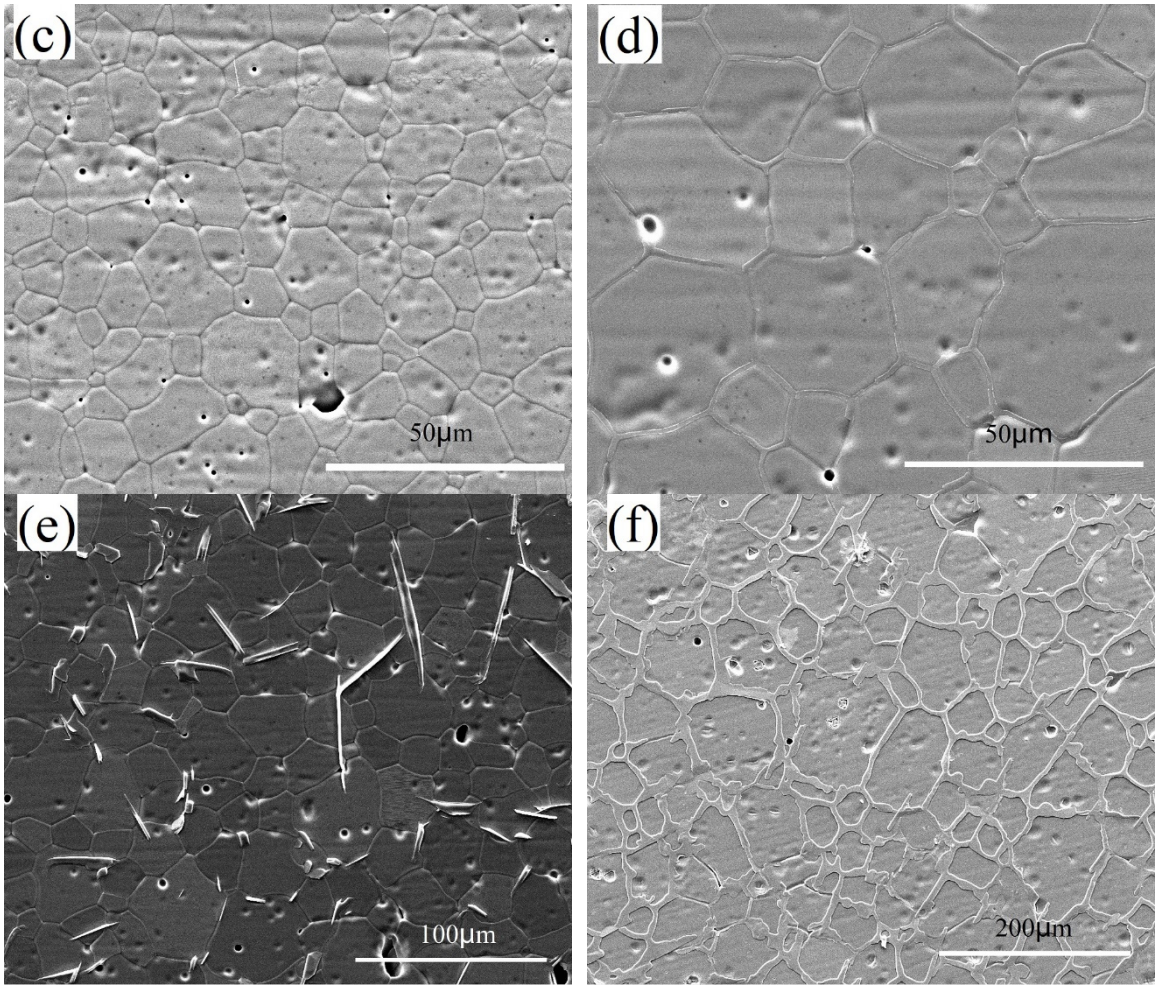

Fig. 5 Cross-section SEM of 0Ti (a, b), 5Ti (c, d), and 10Ti (e, f) pellets sintered at 1500 ℃ for 4 h (a, c, e) and 30h (b, d, f).

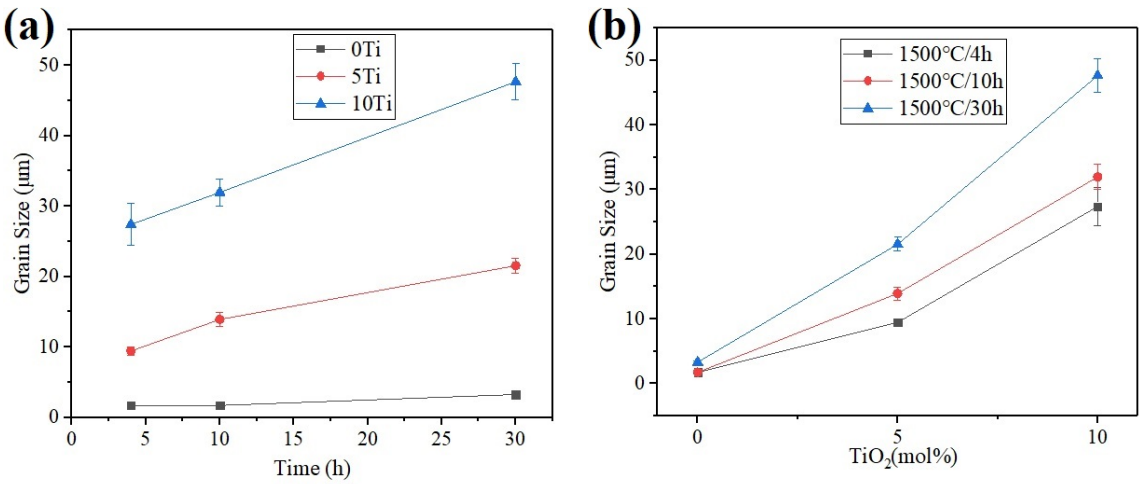

Fig. 6 Grain size(a) vs. sintering time, and (b) vs. TiO_2 content variations of 0Ti, 5Ti, and 10Ti bulk specimens sintered at 1500 ℃ for 4 h, 10 h, and 30 h.

Table 2 Ionic radii and atomic masses of the matrix and dopant elements [26].

Element	La^{3+}	Gd^{3+}	Y^{3+}	Yb^{3+}	Zr^{4+}	Ti^{4+}
Ionic radius (Å)	1.160	1.053	1.019	0.895	0.840	0.740
Atomic mass	138.9	157.3	88.91	173	91.22	47.87

3.4 $La_2Zr_2O_7$ precipitation of sintered pellets

As seen in Fig. 5(e) and (f), precipitations emerged on the surface of the 10Ti specimens after sintering, its size increasing with increasing sintering time. EDS analysis indicated that the precipitations mainly contained La and Ti elements (see Fig. 7), suggesting that these precipitations were the new phase of $La_2Ti_2O_7$ produced. In the 5Ti specimens we also observed very little amount of precipitations of approximately 1-2 um in width at the grain boundaries after 30 h of sintering (see Fig. 5(d)). Although no $La_2Ti_2O_7$ phase was detected in 5Ti pellets sintered for 4 h and 10 h (Fig. 3a), $La_2Ti_2O_7$ precipitation was found in 5Ti pellets sintered for only 4 h, as shown in Fig. 8, which was due to the amount of $La_2Ti_2O_7$ precipitation in these samples is below the lower limit of detection by XRD.

There is only 1 mol% La_2O_3 in all pellets, which means the La_2O_3 stabilizer in pellets is not uniform in microscale or nanoscale so that the formation rate of $La_2Ti_2O_7$ is charged by the diffusion rate of Ti^{4+} in the pellet. Therefore, the content of $La_2Ti_2O_7$ should increase with the increase of TiO_2 content and sintering time. According to the SEM morphologies and XRD patterns of 5Ti and 10Ti sintered pellets, the $La_2Ti_2O_7$ content in 5Ti pellet gradually increases with the increase of the sintering time, and the $La_2Ti_2O_7$ content in 10Ti pellets are much larger than that in 5Ti pellets. However, the content of $La_2Ti_2O_7$ in 10Ti pellets are much higher than its actual content, and the content of $La_2Ti_2O_7$ in 10Ti seems to be gradually decreasing with the increase of sintering time. The (010) preferred orientation of $La_2Ti_2O_7$ may be a reason why its relative diffraction intensity is higher than the actual content, but it does not explain the higher relative area fraction of $La_2Ti_2O_7$ than its actual content. This may be due to the following reasons.

As mentioned above, the high content of TiO_2 means the probability of reaction with La_2O_3 is high, therefore, La_2O_3 rapidly reacted with TiO_2 to form a lot of $La_2Ti_2O_7$ in a 10Ti pellet. According to the literature [27,28], it is known that the vapor pressure of La_2O_3 and TiO_2 is much higher than that of ZrO_2, Y_2O_3, Gd_2O_3 and Yb_2O_3 in the sample. Compared with ZrO_2, the melting point of $La_2Ti_2O_7$ (1790 °C) is much lower, and it is known from the La_2O_3-TiO_2 binary phase diagram [29] that its solid-liquid transition temperature decreases further with the increase of TiO_2 content in a certain range. Therefore, the $La_2Ti_2O_7$ precipitations within the pellet are diffused to the pellet surface by an evaporation-condensation mechanism during sintering at 1500 °C. This is the reason for the protrusion of $La_2Ti_2O_7$ on the surface and thermal etching cross-section of the 10Ti pellet. At the early stage of sintering, the pellet has a lot of grain boundaries and pores, these pores and grain boundaries provide channels for $La_2Ti_2O_7$ near the surface to diffuse to the surface, thus forming a lot of $La_2Ti_2O_7$ on the surface of the pellet. With the increase of sintering time, most of the pores and grain boundaries of the pellet disappeared due to grain growth, resulting in a rapid reduction of the vapor diffusion channels, so it is difficult for the $La_2Ti_2O_7$ inside the pellet to continue to diffuse to the pellet surface, and the relative surface area ratio of $La_2Ti_2O_7$ on the surface also decreases due to the growth of the ZrO_2 grains. This is the reason for the decrease in $La_2Ti_2O_7$ content with increasing sintering time observed in the 10Ti pellet. In addition, since $La_2Ti_2O_7$near the surface can still diffuse to the surface and exhibit a (010) preferred orientation, it still exhibits a higher XRD relative intensity than cubic ZrO_2 even after 30 h.

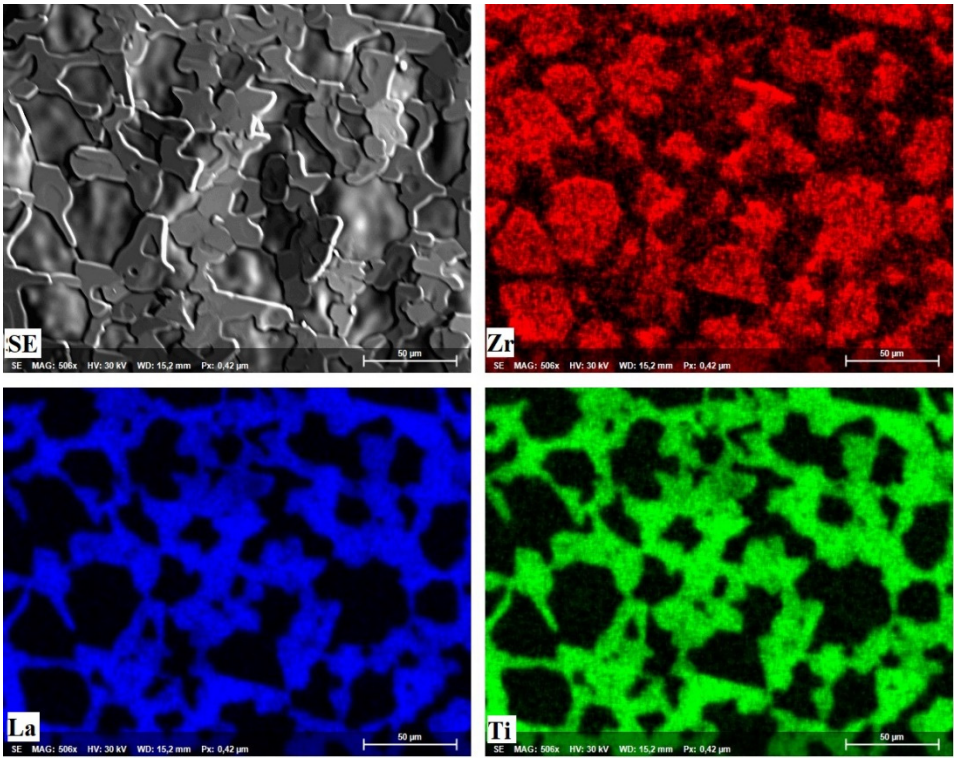

Fig. 7 EDS analysis of 10Ti sintered at 1500 ℃ for 30 h, only Zr, La, and Ti were shown here.

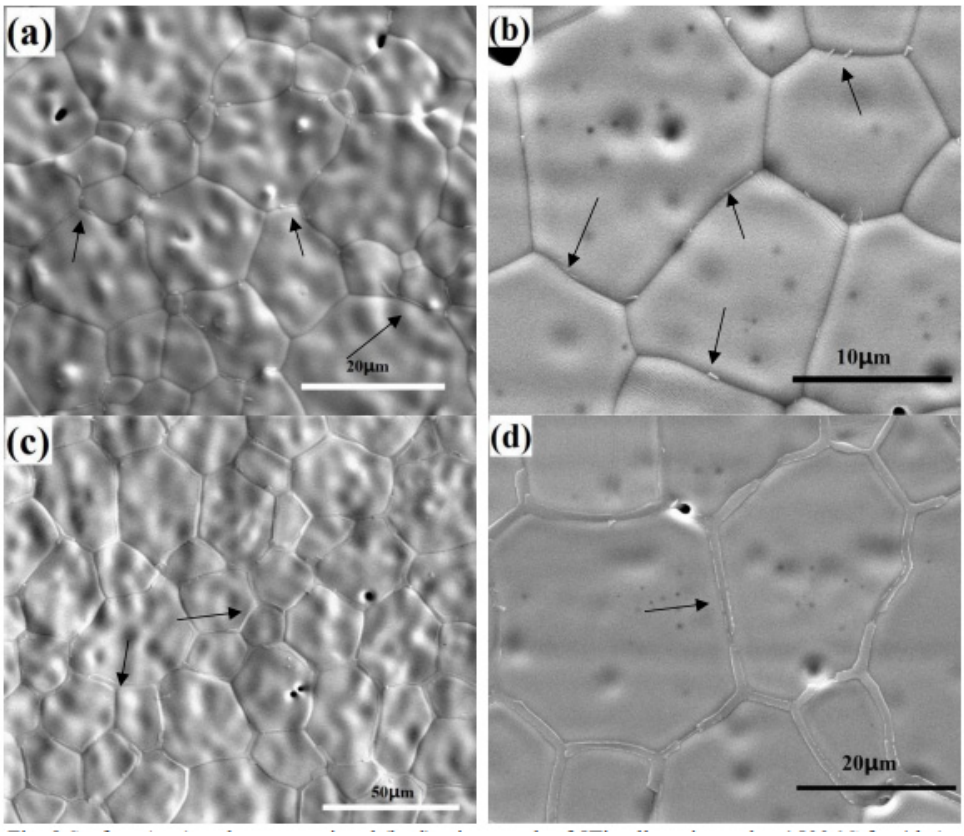

Fig. 8 Surface (a, c) and cross-sectional (b, d) micrograph of 5Ti pellets sintered at 1500 ℃ for 4 h (a, b) and 30 h (c, d). Arrows indicate the new formations.

4. Conclusion

In this paper, the influence of TiO_2 addition (5 and 10 mol%) on phase stability and sintering behavior of 1 mol%La_2O_3-2 mol%Gd_2O_3-2 mol%Yb_2O_3-6 mol%Y_2O_3 co-doped ZrO_2 (LGYYSZ) at 1500 ℃ were studied. The results are as follows:

(1) The addition of TiO_2 lowered the eutectic temperature of LGYYSZ. The specimens doped with 0 mol% of TiO_2 were obtained in complete cubic phase after sintering at 1500 ℃ for 10 h, while the specimens doped with 10 mol% of TiO_2 only required sintering at 1400 °C for 4 h.

(2) The addition of TiO_2 resulted in a denser material with greater sintering shrinkage and lower porosity, and significantly promoted grain growth, with microstructures showing an increase in grain size with increasing TiO_2 content.

(3) The TiO_2 addition is reacted with the La_2O_3 in LGYYSZ to form an orthorhombic $La_2Ti_2O_7$ phase with a (010) preferential orientation perpendicular to the surface, the rate of formation of which is influenced by the rate of diffusion of Ti^{4+} in the pellet. The $La_2Ti_2O_7$ precipitated phase is diffused onto the pellet surface during the sintering process by an evaporation-condensation mechanism.

References

[1] Padture, N.P. (2002) Thermal Barrier Coatings for Gas-Turbine Engine Applications. Science, 296(5566), 280–284.

[2] Noemi Rebollo et al. (2003) Phase stability issues in emerging TBC systems. In Opila, E., Hou P., Maruyama, T., Pieraggi, T., Pieraggi, B., McNallan, M., Shifler, D., Wuchina, E. (Eds.), High Temperature Corrosion and Materials Chemistry IV. Electrochemical Society Proceedings vol. PV-2003-16. pp 431-442.

[3] Robert A. Miller et al. (1981) Phase stability in plasma-sprayed partially stabilized zirconia yttria. In Heuer, A.H., Hobbs, L.W., (Eds.), Science and technology of zirconia, in advances in ceramics, Vol. 3. American Ceramic Society, Columbus, Ohio. pp 241-253.

[4] Jérôme Chevalier et al. (2009) The Tetragonal-Monoclinic Transformation in Zirconia: Lessons Learned and Future Trends., 92(9), 1901–1920.

[5] Shuqi Guo and Yutaka Kagawa. (2007) Isothermal and cycle properties of EB-PVD yttria-partially-stabilized zirconia thermal barrier coatings at 1150 and 1300 ℃. Ceramics International, 33 [3], 373–378.

[6] Jean-Francois Bisson et al. (2000) Thermal Conductivity of Yttria–Zirconia Single Crystals, Determined with Spatially Resolved Infrared Thermography. Journal of American Ceramics Society, 83[8], 1993–1998.

[7] Alban Azzopardi et al. (2004) Influence of aging on structure and thermal conductivity of Y-PSZ and Y-FSZ EB-PVD coatings. Surface and Coatings Technology, 177 –178, 131–139.

[8] Bilge Saruhan et al. (2011) Correlation of thermal conductivity changes with anisotropic nano-pores of EB-PVD deposited FYSZ-coatings. Surface and Coatings Technology, 205(23-24), 5369-5378.

[9] Zhan-Guo Liu et al. (2008) Effect of gadolinia on phase structure and thermal conductivity of ZrO_2–4.5 mol%Y_2O_3 ceramics. Materials Letters, 62(20), 3524–3526.

[10] Dong Chen et al. (2019) Investigation of ternary rare earth oxide-doped YSZ and its high temperature stability. Journal of Alloys and Compounds, 806, 580-586.

[11] Dongming Zhu and Robert A. Miller. (2004) Development of Advanced Low Conductivity Thermal Barrier Coatings. International Journal of Applied Ceramic Technology, 1[1], 86-94.

[12] Mercer, C. et al. (2007) On a ferroelastic mechanism governing the toughness of metastable tetragonal-prime (t') yttria-stabilized zirconia. Proc. R. Soc. A, 463(2081), 1393–1408.

[13] Tobias A. Schaedler et al. (2007) Toughening of Non-transformable t'-YSZ by addition of titania. J. Am. Ceram. Soc., 90[12], 3896–3901.

[14] Meng Zhao et al. (2014) Effect of lattice distortion and disordering on the mechanical properties of

titania doped YSZ. Journal of American ceramic society, 97[5], 1566-1571.
[15] Tiandan Chen et al. (2008) Phase stability, microstructural evolution and room temperature mechanical properties of TiO_2 doped 8 mol% Y_2O_3 stabilized ZrO_2 (8Y-CSZ). Ceramics International, 34(2), 365–370.
[16] Süleyman Tekeli et al. (2007) High-temperature deformation behavior of TiO_2-doped 8 mol%Y_2O_3-stabilized ZrO_2 (8Y-CSZ) under tension and compression. Ceramics International, 33(5), 869–874.
[17] Hidehiro Yoshida et al. (2005) Improvement of high temperature tensile ductility in Cubic ZrO_2 through TiO_2 addition. Scripta Materialia, 52(5), 365–368.
[18] Dongming Zhu and Craig Robinson. (2017) Advanced Thermal Barrier and Environmental Barrier Coating Development at NASA GRC. GRC-E-DAA-TN41357.
[19] Liou, S.S. and Worrell, W.L. (1989) Electrical Properties of Novel Mixed-Conducting Oxides. Applied Physicals A, 49(1), 25-31.
[20] Traqueia, L.S.M. et al. (1997) Structural and Electrical Characterization of Titania-Doped YSZ. Journal of the European Ceramic Society, 17(8), 1019-1026.
[21] Radford, K.C. and Bratton, R.J. (1979) Zirconia electrolyte cells Part 1 Sintering studies. Journal of Materials Science, 14(1), 66-69.
[22] Svoboda, J. et al. (1994) Equilibrium pore surfaces, sintering stresses and constitutive equations for the intermediate and late stages of sintering-I. Computation of equilibrium surfaces. Acta Metallurgica et Materialia, 42(2), 435-443.
[23] Yana Xia et al. (2020) Sintered ZrO_2–TiO_2 ceramic composite and its mechanical appraisal. Ceramics International, 46, 775–785.
[24] Shyh-Lung Hwang et al. (1990) Grain Size Control of Tetragonal Zirconia Polycrystals Using the Space Charge Concept. Journal of American Ceramic society, 73(11), 3269-3277.
[25] Lee, I.G. and Chen, I-W. (1988) Sintering and Grain Growth in Tetragonal and Cubic Zirconia. In Somiya, S., Shimada, M., Yoshimura, M., Watanabe, R. (Eds.), Sintering' 87. Elsevier Applied Science, London, U.K. pp. 340-45.
[26] Shannon, R.D. (1976) Revised effective ionic radii and systematic studies of inter atomic distances in halides and chalcogenides. Acta Crystallgraphica, 32(5), 751-767.
[27] Chandrasekharaiah, M.S. (1967) Volatilities of Refractory Inorganic Compounds. In Margrave, J.H. (Eds.), The Characterization of High Temperature Vapors. John Wiley & Sons, New York. pp 495-507.
[28] Uwe Schulz et al. (2004) Review on advanced EB-PVD ceramic topcoats for TBC applications. International journal of applied ceramic technology, 1(4), 302-315.
[29] Škapin, S.D. et al. (2000) Phase stability and equilibria in the La_2O_3-TiO_2 system. Journal of the European Ceramic Society, 20(8), 1179-1185.